

# Photoregulation of Mass Transport through a Photoresponsive Azobenzene-Modified Nanoporous Membrane

Nanguo Liu,<sup>†</sup> Darren R. Dunphy,<sup>‡</sup> Plamen Atanassov,<sup>†</sup> Scott D. Bunge,<sup>‡</sup> Zhu Chen,<sup>†</sup> Gabriel P. López,<sup>†</sup> Timothy J. Boyle,<sup>‡</sup> and C. Jeffrey Brinker<sup>\*,†,‡</sup>

*Chemical and Nuclear Engineering Department and Center for Micro-Engineered Materials, The University of New Mexico, Albuquerque, New Mexico 87131, and Sandia National Laboratories, MS 1349, Albuquerque, New Mexico 87106*

*Received November 25, 2003; Revised Manuscript Received February 20, 2004*

## ABSTRACT

Photoresponsive nanoporous membranes, composed of monosized pores modified with azobenzene ligands, were prepared on an ITO working electrode using an evaporation-induced self-assembly procedure. They exhibited the size-selective photoregulated mass transport of two ferrocene-based molecular probes through the membrane to the electrode surface as determined using a chronoamperometry technique. The measured oxidative current increased and decreased in response to alternating UV and visible light exposure correlating strongly with the photoisomerization state of the azobenzene ligands. This indicates that the optically switchable conformation (trans or cis) of azobenzene ligands controls the effective pore size and, correspondingly, transport behavior on the nanoscale.

Materials that respond predictably to pH,<sup>1–3</sup> temperature,<sup>4,5</sup> light,<sup>6–8</sup> biomolecules,<sup>9–11</sup> or electric fields<sup>12,13</sup> are of potential interest for applications in microfluidics, microvalves, controlled drug release, sensors, optical switches, photomemories, light-driven displays, optical storage, and optomechanical actuation. For example, pH-responsive hydrogels have been integrated into fluidic devices where their volumetric response to pH was used to control flow.<sup>1–3</sup> However, in this case the hydrogel valves were defined on the micrometer scale (using soft lithography), and the response was controlled with macroscale precision. Here we describe a nanocomposite architecture with the potential to control pore size and, correspondingly, transport behavior, with nanometer-scale precision. Our approach exploits the well-known responses of azobenzene ligands to light and heat.<sup>7,8,14–17</sup> Trans ↔ cis isomerization of azobenzene moieties changes not only the molecular dimension (molecular length of the cis isomer is ca. 3.4 Å shorter than that of the trans isomer on the basis of a molecular simulation using ChemBats3D Pro 5.5 software) but also the dipole moment (0.5–3.1 D). For materials incorporating noncovalently bonded azobenzene ligands, these switchable properties have been used to control the gas permeation of a microporous

zeolite membrane,<sup>18</sup> to change the *d* spacing of intercalated nanocomposites,<sup>19</sup> to direct the self-assembly of supramolecular structures in trans or cis forms,<sup>20</sup> and to control the flux of a synthetic ion channel.<sup>21</sup>

However, to best utilize photoisomerization to control pore size accurately, we need to anchor azobenzene ligands to the pore surfaces of a nanostructured scaffold composed of monosized pores. This allows the rigid inorganic scaffold to position azobenzene ligands precisely in nanostructured 3D configurations where switching results in a well-defined change in pore size. (See Figure 1.) The 3D composite architecture should also enhance the mechanical and thermal stability of the switchable ligands, which is important for their integration into devices.

Surfactant-directed self-assembly<sup>22–25</sup> has been extended to form films with monosized pores and controlled surface chemistries. Recently we reported a photoresponsive nanocomposite thin film formed by (evaporation-induced) surfactant-directed self-assembly (EISA) of an azobenzene-modified silane, 4-(3-triethoxysilylpropylureido)azobenzene (TSUA) and tetraethyl orthosilicate (TEOS).<sup>26</sup> In EISA, the amphiphilic hydrolyzed TSUA molecules function as cosurfactants, positioning hydrophobic propylureidoazobenzene groups in the hydrophobic micellar cores and co-organizing the hydrophilic silicic acid groups with hydrolyzed TEOS moieties at the hydrophilic micellar exteriors. After catalyst

\* Corresponding author. E-mail: cjbrink@sandia.gov.

<sup>†</sup> University of New Mexico.

<sup>‡</sup> Sandia National Laboratory.

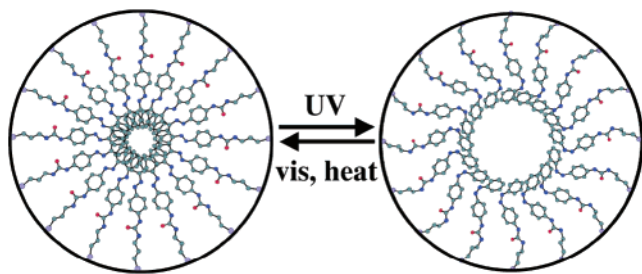


**Figure 1.** Schematic drawing of the reversible change in size of azobenzene-modified pores in response to environmental stimuli (light or heat). The trans or cis conformation of the azobenzene ligands was calculated using ChemBats3D Pro molecular modeling analysis software. Surface coverage was calculated on the basis of the surface area and weight loss of the nanoporous film. Atomic legend: gray (C), red (O), dark blue (N), blue (Si); H atoms are omitted.

or thermally promoted siloxane condensation, TSUA is anchored to the surfaces of monosized pores with the azobenzene ligands disposed toward the pore interiors. (See Figure 1.) The as-synthesized crack-free thin films (~260 nm in thickness) showed not only a highly ordered mesostructure but also a reversible photoresponse to alternate UV and room light exposures as monitored by UV/vis spectroscopy.

Herein we report on our continuing investigation of the mesostructure and function of a photoresponsive nanocomposite film using transmission electron microscopy (TEM), 2D grazing incidence small-angle X-ray scattering (GISAXS), and electrochemical methods. We show for the first time optically mediated control of mass transport in a self-assembled inorganic nanocomposite.

Figure 2 shows a representative TEM cross-sectional image of an as-prepared photoresponsive nanocomposite film, which exhibits a highly ordered cubic mesostructure. The average center-to-center pore spacing is 5.6 nm. The 2D GISAXS data (Figure 2 inset) confirms that the pores are arranged in a body-centered cubic mesostructure (bcc,  $Im\bar{3}m$  space group) with a unit cell dimension of  $a = 5.7$  nm ( $d_{200} = 2.85$  nm). The 2D GISAXS data indicates that the (100) plane of the bcc mesostructure is oriented parallel to the silicon substrate. The slight distortion of the bcc mesostructure is due to the greater shrinkage in the direction normal to the substrate than parallel to the substrate resulting from laterally constrained siloxane condensation.

As illustrated in Figure 1, we expect the azobenzene-functionalized nanocomposite films to have optically switchable effective pore sizes. Under UV irradiation, isomerization of the azobenzene ligands from the thermodynamically stable trans form to the metastable cis form causes their retraction, increasing the pore size and thus the mass transport rate through the nanocomposite films. Exposure to lower-energy radiation or heat has the reverse effect.

To demonstrate optical control of mass transport, we performed a chronoamperometry experiment using an azobenzene-functionalized nanocomposite membrane to modify the working electrode in an electrochemical cell. See the setup in Figure 3. The chronoamperometry experiment uses

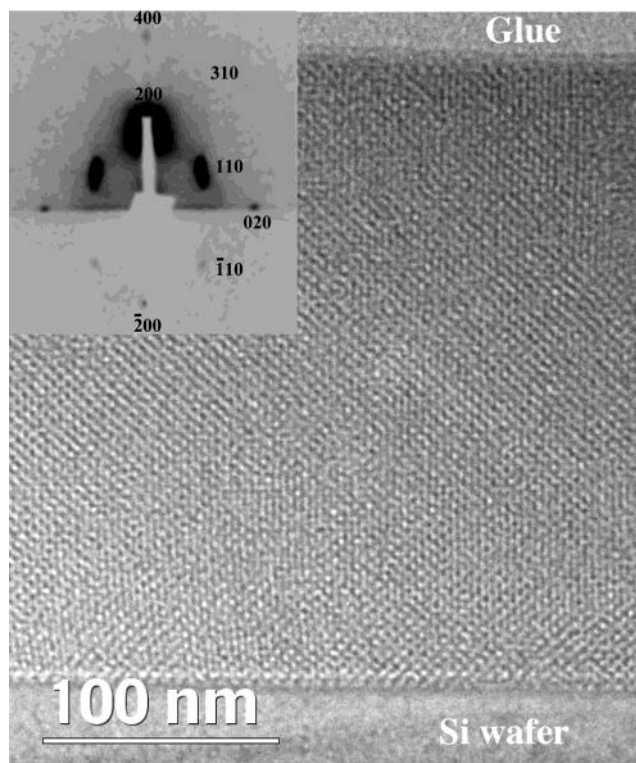


**Figure 2.** Cross-sectional TEM image of a photoresponsive nanoporous film. Inset is a 2D GISAXS pattern shown in reverse grayscale. The lower half of the plane is in the shadow of the silicon substrate, and the scattering spots are attenuated.

ferrocene dimethanol (FDM,  $\text{Fe}(\text{C}_5\text{H}_5\text{CH}_2\text{OH})_2$ ) or ferrocene dimethanol diethylene glycol (FDMDG,  $\text{Fe}(\text{C}_5\text{H}_5\text{CH}_2(\text{OCH}_2\text{CH}_2)_2\text{OH})_2$ ) as a molecular probe and provides a measure of mass transport through the nanocomposite membrane by monitoring the steady-state oxidative currents at constant potential for the reactions (Scheme 1) taking place on the working electrode surface (indium tin oxide, ITO). At constant potential, the effective pore size limits the diffusion rate of probing molecules to the electrode surface during electrolysis. (Because FDM and FDMDG are uncharged molecules, the electromigration effect can be ignored.) Under dark conditions, the azobenzene moieties are predominately in their extended trans form. Upon UV irradiation ( $\lambda = 360$  nm), the azobenzene moieties isomerize to the more compact cis form, which should increase the diffusion rate and correspondingly the oxidative current. Exposure to visible light ( $\lambda = 435$  nm) triggers cis  $\rightarrow$  trans isomerization of the azobenzene moieties, decreasing the current to the pre-UV exposure level.

In a typical chronoamperometry experiment performed using a potentiostat (BioAnalytical Systems, model CV-50W), photoresponsive nanocomposite membranes were spin-coated onto an ITO substrate that was mounted in a homemade electrochemical flow cell as a working electrode (WE). A Ag/AgCl reference electrode (RE) and a Pt counterelectrode (CE) were placed in a solution containing 1 mM FDM (or FDMDG) and electrolyte (10 mM pH 7.0 tris buffer + 50 mM KCl). A peristaltic pump was used to pump fresh solution into the cell and to help maintain steady-state concentration profile conditions at the surface of the

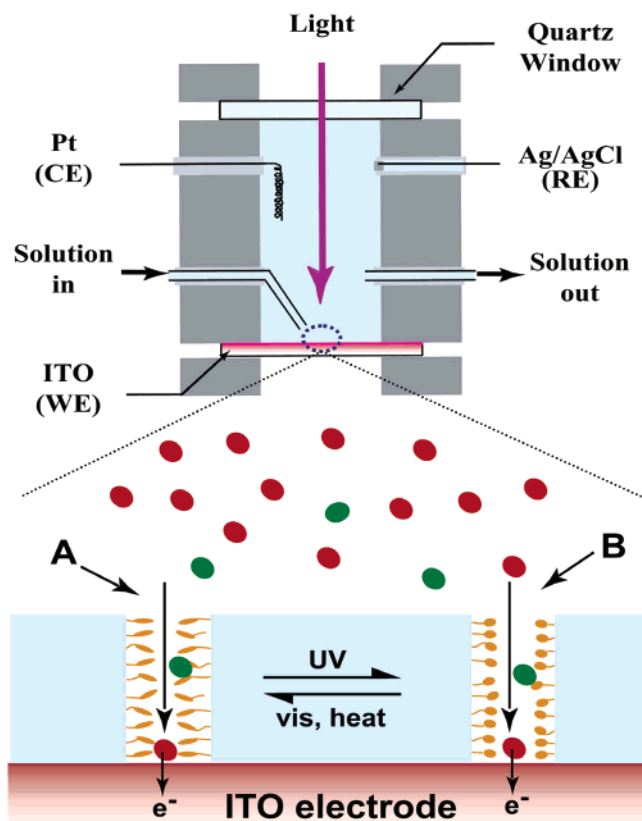
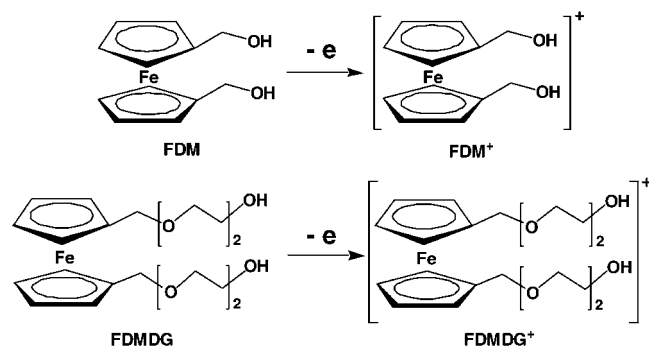


**Figure 3.** Schematic drawing of the electrochemical cell (top) and mass transport of probing molecules through the photoresponsive nanocomposite membrane integrated on an ITO electrode (bottom). (A) Diffusion through smaller pores with azobenzene ligands in their trans configuration; (B) diffusion through larger pores with azobenzene ligands in their cis configuration. Legend: red ovals (FDM or FMDG<sup>+</sup>), green ovals (FDM<sup>+</sup> or FMDG<sup>+</sup>), orange ovals (azobenzene in cis form), orange elongated oval (azobenzene in trans form).

**Scheme 1.** Electrochemical Reactions Taking Place on the ITO Working Electrode Surface



working electrode. One end of the cell was a quartz window, designed to allow the illumination of the working electrode with UV or visible light and acquisition. The cell was placed in a Faraday cage made of copper mesh to screen the magnetic and electrical noise. A Hg–Xe arc lamp (ORIEL, model 66002) with a fiber optic was used as the light source. Optical filters were used to select UV (360 nm, band pass) or visible (435 nm, long pass) light.

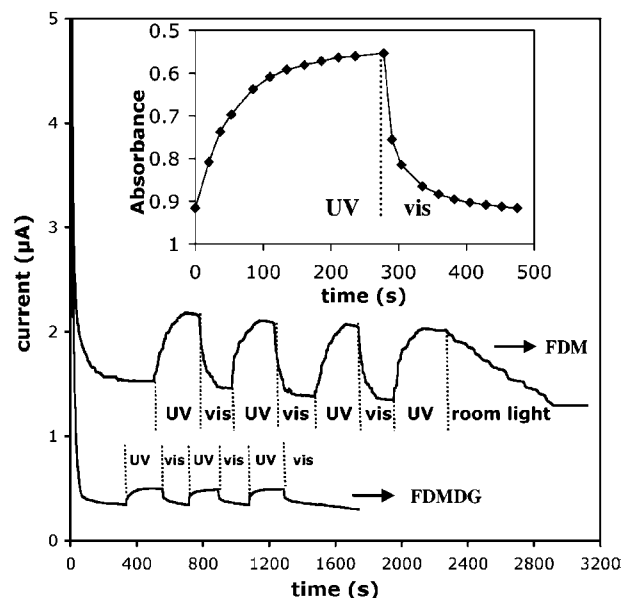


**Figure 4.**  $I-t$  behavior of a photoresponsive nanocomposite film under alternate exposure to UV (360 nm) and visible light (435 nm). (Last cycle uses room light, 400–700 nm.) Inset is the absorbance at 356 nm ( $\pi-\pi^*$  transition of the trans isomer) of the same film immersed in the buffer solution containing 1 mM FDM. The time scale of the UV/vis data corresponds to that of the first cycle in the  $I-t$  response curve using FDM as the molecular probe.

Figure 4 shows typical current–time photoresponses of the membrane-modified electrode measured at a constant potential of 650 mV. In the curve using FDM as the molecular probe, we observed that after an initial decay due to electrode charging and the formation of a depletion layer of FDM through the membrane the oxidative current of FDM reaches the steady state after about 360 s. Upon UV ( $\lambda = 360$  nm) irradiation, the current increases progressively because of trans  $\rightarrow$  cis isomerization, which increases the pore size before reaching a new plateau after 270 s, corresponding to the photostationary state of trans  $\rightarrow$  cis isomerization. Visible light ( $\lambda = 435$  nm) exposure decreases the oxidative current due to cis  $\rightarrow$  trans isomerization, which decreases the pore size. After 200 s of this light exposure, the current is reduced to its pre-UV exposure level, corresponding to the photostationary state of cis  $\rightarrow$  trans isomerization. Three cycles of alternating UV/visible light exposure were performed to show the reversibility and repeatability of this process. In the last cycle, much weaker visible light (0.5 mW) was used instead of stronger visible light (5.6 mW). We observed a much slower decrease in current, demonstrating the slower response under lower illumination levels. Control experiments were performed on a bare ITO electrode and a mesoporous silica-coated ITO electrode (2.5-nm pore diameter). However, no photoresponse was observed in either of these systems, demonstrating that the photoresponse in the present electrode/film architecture is not an artifact of the ITO electrode or the mesoporous silica film but is a true effect due to the isomerization of azobenzene moieties attached to the nanopore surfaces.

To correlate the observed current changes with the actual isomerization state, a UV/vis spectroscopy study was per-

formed in which the nanocomposite film used for chronoamperometry was immersed in the electrolyte solution and illuminated exactly as for the first  $I-t$  cycle in the chronoamperometry experiment using FDM as the molecular probe. As shown in the inset of Figure 4, the absorbance of the nanocomposite film at 356 nm ( $\lambda_{\text{max}}$  of the  $\pi-\pi^*$  transition of azobenzene in the trans form) decreases progressively under UV ( $\lambda = 360$  nm) irradiation and reaches a plateau, which corresponds to the photostationary state of trans  $\rightarrow$  cis isomerization. The following visible light ( $\lambda = 435$  nm) exposure causes the reverse cis  $\rightarrow$  trans isomerization, increasing the absorbance gradually before reaching the pre-UV state. This data exactly correlates the conformational changes of azobenzene moieties in the nanocomposite film with the oxidative current changes measured in the chronoamperometry experiment. This demonstrates for the first time optical control of mass transport through a nanocomposite thin film.

To investigate the influence of the size of the probing molecules on mass transport, we synthesized FDMDG according to a previously reported procedure<sup>27</sup> and performed a chronoamperometry experiment using FDMDG as the molecular probe. The  $I-t$  curve (Figure 4) of the photoresponsive nanocomposite film shows similar photoresponses to that of the FDM probe (i.e., the oxidative current increases under UV light (360 nm) irradiation and decreases under visible light (435 nm) exposure). For FDM and FDMDG probes, the ratios of maximum current change to the original steady-state current are 40% ( $0.62 \mu\text{A}/1.54 \mu\text{A}$ ) and 47% ( $0.16 \mu\text{A}/0.34 \mu\text{A}$ ), respectively. As calculated using CS Chem 3D Pro software, the Connolly solvent-excluded volumes of FDM and FDMDG are 269 and 392  $\text{\AA}^3$ , respectively. From Figure 4, it is apparent that increasing the volume of the probe molecule lowers the overall mass transport, thereby decreasing the oxidative current, but increases the selectivity as evidenced by the greater normalized current ratio. Current work is investigating changing the overall pore size or probe size to demonstrate “on/off” control with these nanovalves.

In conclusion, we showed that ordered azobenzene-functionalized nanoporous films prepared as supported membranes exhibit dynamic photocontrol of their pore size, which in turn enables the photoregulation of mass transport. We can anticipate their potential applications in nanofluidic devices, nanovalves, nanogates, smart gas masks, membrane separation, and controlled release.

**Acknowledgment.** This work was supported by the Air Force Office of Scientific Research Award Number F49620-01-1-0168, the DOD MURI Program Contract 318651, the DOE Office of Basic Energy Sciences Molecular Nanocom-

posite Program and NSET Program DEFG03-02ER15368, and the SNL Lab Directed Research and Development Program. Sandia National Laboratories (SNL) is a Lockheed Martin Company operated by the U.S. Department of Energy under contract DE-AC04-94AL85000. We appreciate the help from Jin Wang at Argonne National Laboratory in performing the GISAXS experiment and the technical support from the TEM Imaging Center of the Earth and Planetary Science Department at the University of New Mexico supervised by Dr. Huifang Xu.

## References

- (1) Beebe, D. J.; Moore, J. S.; Bauer, J. M.; Yu, Q.; Liu, R. H.; Devadoss, C.; Jo, B.-H. *Nature* **2000**, *404*, 588.
- (2) Yu, Q.; Bauer, J. M.; Moore, J. S.; Beebe, D. J. *Appl. Phys. Lett.* **2001**, *78*, 2589.
- (3) Liu, R. H.; Yu, Q.; Beebe, D. J. *J. Microelectromech. Syst.* **2002**, *11*, 45.
- (4) Yoshida, R.; Uchida, K.; Kaneko, Y.; Sakai, K.; Kikuchi, A.; Sakurai, Y.; Okano, T. *Nature* **1995**, *374*, 240.
- (5) Garnweitner, G.; Smarsly, B.; Assink, R.; Ruland, W.; Bond, E.; Brinker, C. J. *J. Am. Chem. Soc.* **2003**, *125*, 5626.
- (6) Mal, N. K.; Fujiwara, M.; Tanaka, Y. *Nature* **2003**, *421*, 350.
- (7) Rau, H. In *Photochemistry and Photophysics*; Rabek, J., Ed.; CRC Press: Boca Raton, FL, 1990; Vol. 2, Chapter 4.
- (8) Natansohn, A. In *Macromolecular Symposia*; Höcker, H.; Guth, W.; Jung, B.; Meisel, I.; Spiegel, S., Eds.; Wiley-VCH Verlag: Weinheim, Germany, 1999; p 1.
- (9) Kataoka, K.; Miyazaki, H.; Bunya, M.; Okano, T.; Sakurai, Y. *J. Am. Chem. Soc.* **1998**, *120*, 12694.
- (10) Kokufuta, E.; Zhang, Y. Q.; Tanaka, T. *Nature* **1991**, *351*, 302.
- (11) Miyata, T.; Asami, N.; Uragami, T. *Nature* **1999**, *399*, 766.
- (12) Tanaka, T.; Nishio, I.; Sun, S. T.; Uenonishio, S. *Science* **1982**, *218*, 467.
- (13) Kwon, I. C.; Bae, Y. H.; Kim, S. W. *Nature* **1991**, *354*, 291.
- (14) Kumar, G. S.; Neckers, D. C. *Chem. Rev.* **1989**, *89*, 1915.
- (15) Ueda, M.; Kim, H.-B.; Ichimura, K. *Chem. Mater.* **1994**, *6*, 1771.
- (16) Kozlecki, T.; Wilk, K. A.; Gancarz, R. *J. Photochem. Photobiol., A* **1998**, *116*, 229.
- (17) Liu, N. G.; Dunphy, D. R.; Rodriguez, M. A.; Singer, S.; Brinker, C. J. *Chem. Commun.* **2003**, 1144.
- (18) Weh, K.; Noack, M.; Hoffmann, K.; Schröder, K.-P.; Caro, J. *Microporous Mesoporous Mater.* **2002**, *54*, 15.
- (19) Ogawa, M.; Ishii, T.; Miyamoto, N.; Kuroda, K. *Adv. Mater.* **2001**, *13*, 1107.
- (20) Liu, N. G.; Yu, K.; Smarsly, B.; Dunphy, D. R.; Jiang, Y.-B.; Brinker, C. J. *J. Am. Chem. Soc.* **2002**, *124*, 14540.
- (21) Kobuke, Y.; Ohgoshi, A. *Colloids Surf., A* **2000**, *169*, 187–197.
- (22) Kresge, C. T.; Leonowicz, M. E.; Roth, W. J.; Vartuli, J. C.; Beck, J. S. *Nature* **1992**, *359*, 710.
- (23) Lu, Y.; Ganguli, R.; Drewien, C. A.; Anderson, M. T.; Brinker, C. J.; Gong, W. L.; Guo, Y. X.; Soyez, H.; Dunn, B.; Huang, M. H.; Zink, J. I. *Nature* **1997**, *389*, 364.
- (24) Lu, Y.; Fan, H.; Stump, A.; Ward, T. L.; Reiker, T.; Brinker, C. J. *Nature* **1999**, *398*, 223.
- (25) Feng, X.; Fryxell, G. E.; Wang, L.-Q.; Kim, A. Y.; Liu, J.; Kemner, K. M. *Science* **1997**, *276*, 923.
- (26) Liu, N. G.; Chen, Z.; Dunphy, D. R.; Jiang, Y.-B.; Assink, R. A.; Brinker, C. J. *Angew. Chem., Int. Ed.* **2003**, *42*, 1731.
- (27) Lindner, E.; Kehrer, U.; Steimann, M.; Ströbele, M. *J. Organomet. Chem.* **2001**, *630*, 266.

NL0350783